DYNAMICS OF FREE-FIXED PLANAR SERIAL MECHANISMS WITH RIGID LINKS AND FLEXIBLE HINGES

NICOLAE LOBONȚIU[1], SIMONA NOVEANU[2], DAN NOVEANU[2]

Abstract. A lumped-parameter dynamic model is developed for planar serial mechanisms with free-fixed ends and comprising rigid links connected to flexible hinges. Based on the rigid links degrees of freedom, the method assembles a mass matrix accounting for both rigid links and flexible hinges inertia, as well as an exact compliance matrix that considers both bending and axial deformations of the hinges. The two matrices are utilized to calculate the in-plane natural frequencies and mode shapes via the dynamic matrix, and to predict the free or forced time response of the mechanism. The dynamics of a particular collinear mechanism, formed of two rigid links and two flexible hinges, are thoroughly analyzed in terms of geometric parameters, and by also including the gravity effects when the mechanism is vertical and behaves as a double pendulum.

Key words: mechanism, serial, flexible hinge, rigid link, compliance, inertia, lumped parameters, natural frequency, dynamics, double pendulum.

1. INTRODUCTION

Monolithic mechanisms that are constructed by serially connecting rigid links (the members that perform mechanical work and carry the payload) and flexible hinges (the compliant joints) are amply utilized in a wide range of applications including flexible robotics, precision positioning, manipulation and machining, displacement-amplification mechanisms, orthotic/medical devices, flexible surgical robotics, sensing/actuation, fiber optics, telecommunications, microelectronics, and micro/nano electromechanical systems.

The dynamic behavior of these mechanisms is typically studied with approaches pertaining to the flexible multibody systems [1–2]. The finite element analysis (FEA) is one of the methods utilized to model and solve multibody system dynamics problems [3–9]. For free systems, FEA leads to linear eigenvalue formulations where the mass and stiffness matrices are calculated separately. Aside from requiring a relatively large number of degrees of freedom (DOF), a particular

[1] University of Alaska Anchorage, USA
[2] Universitatea Tehnică din Cluj-Napoca, Romania

Ro. J. Techn. Sci. − Appl. Mechanics, Vol. 70, N^{os} 1–3, P. 5–21, Bucharest, 2025

DOI:10.59277/RJTS-AM.2025.1-3.01

drawback of the method results from the discrepancy in elastic properties between the rigid and the flexible links that may generate ill-conditioned mathematical models and, therefore, inaccurate results. Another technique for modeling the dynamics of multibody systems is the dynamic stiffness matrix method [10–12], which employs a smaller number of DOF than FEA and formulates a matrix (the dynamic stiffness matrix) directly in the frequency domain, and whose determinant provides the eigenvalues. The transfer matrix method [13–16] simplifies the dynamic stiffness matrix method by further reducing the number of DOF and using an algebraic transfer algorithm for the solution. Both the dynamic stiffness matrix and the transfer matrix methods result in transcendental eigenvalue problems that require numerical algorithms to find the solution [17, 18]. Another multibody system mathematical modeling category includes symbolic techniques coupled with numerical solution algorithms that are usually sourced in distributed-parameter models [19–21]. Methods and algorithms aimed at reducing the number of DOF and at simplifying the mathematical models of multibody systems have also been developed, as discussed in [22–24].

A lumped-parameter analytic model is formulated here to describe the in-plane dynamics of planar mechanisms that are designed as serial chains with one end free and the other end fixed, and that combine rigid links with flexible hinges [25]. The model is general and can be applied to any mechanism structure, flexible hinge configurations, and number of links. The number of DOF is inherently minimum because they represent the in-plane motion coordinates of all the rigid links' mass centers. Based on these DOF, a mass matrix is assembled that includes the inertia of both the heavy rigid links and the flexible hinges. Consistent with the mass matrix, an exact compliance matrix is separately assembled by collecting all flexible hinges' elastic properties related to both bending and axial small deformations. Utilizing compliances instead of stiffnesses in a serial architecture presents the advantages of simply using zero compliances for rigid links and of algebraically adding compliances for the linear analysis. The mass and compliance matrices are utilized to calculate the dynamic matrix, which results in a linear eigenvalue problem that provides the natural frequencies and the associated mode shapes. The same matrices can also be used to formulate and solve the time-domain free/forced response of the mechanism.

The general mathematical model is applied to the specific design of a collinear mechanism with two rigid links and two flexible hinges of constant cross-section. The mechanism can be positioned either in a horizontal plane (case where gravitational effects are eliminated) or along a vertical axis (with the gravitational action being accounted for) when the mechanism becomes a double pendulum. The natural frequencies of the horizontal-plane mechanism are calculated for both massless and heavy hinges. It is shown that for typical designs with small-dimension (and therefore light) hinges, the inertia of the heavy rigid links is dominant, which enables to ignore the hinges' inertia without affecting the accuracy of the calculated natural frequencies. The analytic-model natural frequencies and mode shapes are confirmed by those obtained with finite element simulation. The influence of the geometric parameters on the natural frequencies' values is also investigated. The gravitational effects in the double pendulum slightly modify the compliance matrix without substantially altering the natural frequencies. The time response of the double pendulum under the action of the gravitational forces is evaluated by means of the modal superposition method.

2. GENERAL ANALYTICAL MODEL

The planar serial chain of Fig. 1 is a sequence of n rigid links and n flexible hinges that starts with a free rigid link and ends with a fixed flexible hinge. It is assumed that the rigid links are heavy, whereas the flexible hinges (whose primary function is to allow relative motion/rotation between neighbouring rigid links) are light (massless at limit). Based on the system's DOF corresponding to the in-plane motion, a mass matrix and a compliance matrix are formed separately. The two matrices enable to calculate the dynamic matrix, which results in a linear eigenvalue problem providing the system's natural frequencies. For external forcing, the time response of the serial chain is evaluated by means of the modal superposition method.

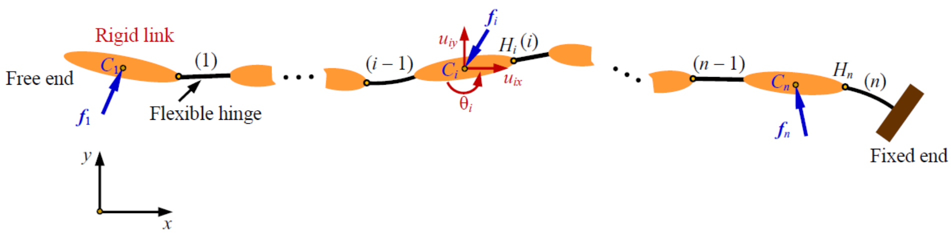

Fig. 1 – Free-end, fixed-end planar serial mechanism with multiple rigid links and flexible hinges.

The method proposed here establishes the system's DOF based on the rigid links of the serial mechanism. Each rigid link has three DOF that describe its position in the xy plane. For the rigid link i, the x and y displacements u_{ix}, u_{iy}, and the z-axis rotation θ_i related to the link mass center C_i are collected in the displacement vector $\boldsymbol{u_i} = [u_{ix}\ \ u_{iy}\ \ \theta_i]^T$ – see Fig. 1. Consequently, the serial mechanism of Fig. 1, which comprises n rigid links and an equal number of flexible hinges, has $3n$ DOF; the DOF define the overall displacement vector $\boldsymbol{u} = [\boldsymbol{u_1}\ \ \boldsymbol{u_2} \ldots \boldsymbol{u_i} \ldots \boldsymbol{u_n}]^T$.

Mass and compliance matrices

Consistent with the DOF associated to the mass centers of the n rigid links, a mass matrix $\mathbf{M}$ is assembled that mainly accounts for the inertia of the rigid heavy links. Inertia contributions from the flexible links can also be added to the rigid links inertia when the hinge mass is not negligible. The diagonal $3n \times 3n$ matrix **M** is formed of the 3 x 3 submatrices $\mathbf{M}^{(i)}$ that are associated to the rigid links centers C_i as follows:

$$\operatorname{diag}\mathbf{M} = \begin{pmatrix} \mathbf{M}^{(1)} & \mathbf{M}^{(2)} & \ldots & \mathbf{M}^{(i)} & \ldots & \mathbf{M}^{(n)} \end{pmatrix}$$
$$\text{with} \quad \mathbf{M}^{(i)} = \begin{bmatrix} m_i & 0 & 0 \\ 0 & m_i & 0 \\ 0 & 0 & J_i \end{bmatrix} \tag{1}$$

where m_i is the lumped mass and J_i is the z-axis mass moment of inertia of the rigid link, both located at C_i; $i = 1, 2, \ldots, n$. The mass m_i is either the rigid link mass only (when the flexible hinges are light and considered massless) or adds lumped fractions of the adjacent flexible links masses to the rigid link mass (when the flexible hinge mass cannot be eliminated) – full details on how to evaluate m_i in this latter instance are discussed for a specific mechanism in Section 3.

Considering that a force vector $\boldsymbol{f} = [\boldsymbol{f}_1 \ \boldsymbol{f}_2 \ldots \boldsymbol{f}_i \ldots \boldsymbol{f}_n]^T$, formed of 3-component vectors $\boldsymbol{f}_i$ applied at the rigid links centers C_i (see Fig. 1), acts on the mechanism, the displacement vector $\boldsymbol{u}$ and the force vector $\boldsymbol{f}$ are connected by means of the compliance matrix **C** as $\boldsymbol{u} = \mathbf{C}\boldsymbol{f}$. Each flexible hinge is defined by a 3×3 compliance matrix $\mathbf{C}^{(i)}$ whose analytically calculated components are available in the literature for typical hinge configurations. Given the serial structure of the mechanism, the overall/assembled compliance matrix **C** is obtained by adding the hinge compliance matrices $\mathbf{C}^{(i)}$ after proper transfer to the rigid links centers C_i by following a procedure that is explained in detail for a specific mechanism in Section 3 in this paper. Symbolically, the matrix **C** is assembled as:

$$\mathbf{C} = \begin{bmatrix} \sum_{i=1}^{n} \mathbf{C}_{C_1H_i}^{(i)} & \sum_{i=2}^{n} \mathbf{C}_{C_1H_i}^{(i)} & \ldots & \mathbf{C}_{C_1H_n}^{(n)} \\ \left(\sum_{i=2}^{n} \mathbf{C}_{C_1H_i}^{(i)}\right)^T & \sum_{i=2}^{n} \mathbf{C}_{C_2H_i}^{(i)} & \ldots & \mathbf{C}_{C_2H_n}^{(n)} \\ \ldots & \ldots & \ldots & \ldots \\ \left(\mathbf{C}_{C_1H_n}^{(n)}\right)^T & \left(\mathbf{C}_{C_2H_n}^{(n)}\right)^T & \ldots & \mathbf{C}_{C_nH_n}^{(n)} \end{bmatrix} \quad \text{with}$$
$$\mathbf{C}^{(i)} = \begin{bmatrix} C_x^{(i)} & 0 & 0 \\ 0 & C_{yy}^{(i)} & C_{y\theta}^{(i)} \\ 0 & C_{y\theta}^{(i)} & C_{\theta\theta}^{(i)} \end{bmatrix} \tag{2}$$

and $i = 1, 2, \ldots, n$. $C_x^{(i)}$ is the axial compliance, while $C_{yy}^{(i)}$, $C_{y\theta}^{(i)}$, $C_{\theta\theta}^{(i)}$ are bending-related compliances (whose equations are available). In Eq. (2), $\mathbf{C}_{C_1H_i}^{(i)}$, for instance, is the matrix resulting after translating the original compliance matrix $\mathbf{C}^{(i)}$ of hinge i (which is calculated with respect to point H_i, see Fig. 1) from H_i to C_1.

Natural frequencies and eigenvectors

The following matrix differential equation (see [25], [26], [27]) governs the in-plane free dynamics of the serial mechanism with $3n$ DOF:

$$\mathbf{M}\ddot{\boldsymbol{u}} + \mathbf{K}\boldsymbol{u} = \mathbf{0} \ \text{ or } \ \ddot{\boldsymbol{u}} + \mathbf{D}\boldsymbol{u} = \mathbf{0} \ \text{ with } \ \mathbf{K} = \mathbf{C}^{-1}, \mathbf{D} = \mathbf{M}^{-1}\mathbf{K} = (\mathbf{CM})^{-1}, \tag{3}$$

where **K** is the stiffness matrix (the inverse of the compliance matrix **C**), and **D** is the dynamic matrix. Eq. (3) can be derived by several methods, including Newton's second law of motion or Lagrange's equations. As per the theory of differential equations, the solution $\boldsymbol{u} = \boldsymbol{U}\sin(\omega_n t + \varphi)$ of Eq. (3) leads to the eigenvalue problem:

$$\mathbf{D}\boldsymbol{U} = \lambda_n \boldsymbol{U}, \tag{4}$$

where λ_n is an eigenvalue of **D** and $\boldsymbol{U}$ is the eigenvector corresponding to $\lambda_n = \omega_n^2$, where ω_n is the natural frequency. The signs and values of an eigenvector components describe the mode shape, which illustrates the specific way in which the system's independent coordinates (DOF) combine during the free vibration at any natural frequency.

Time response

The time response (either free or forced) of the undamped mechanism can be found by several methods, including the modal superposition method, which is utilized here. A transformation $\boldsymbol{u} = \mathbf{V}\boldsymbol{v}$, where $\boldsymbol{v}$ is the new-variable vector and **V** is the matrix whose columns are the eigenvectors of **D**, transforms the original forced-system differential equation into:

$$\ddot{\boldsymbol{u}} + \mathbf{D}\boldsymbol{u} = \boldsymbol{f} \ \xrightarrow{\boldsymbol{u}=\mathbf{V}\boldsymbol{v}} \ \ddot{\boldsymbol{v}} + \mathbf{\Lambda}\boldsymbol{v} = \boldsymbol{f}_v \ \text{ with } \ \mathbf{\Lambda} = \mathbf{V}^{-1}\mathbf{D}\mathbf{V}, \quad \boldsymbol{f}_v = \mathbf{V}^{-1}\boldsymbol{f}, \tag{5}$$

where the diagonal spectral matrix $\mathbf{\Lambda}$ comprises the eigenvalues λ_n and $\boldsymbol{f}_v$ is the transformed counterpart of the original forcing vector $\boldsymbol{f}$. For the mechanism of Fig. 1, the transformed matrix Eq. (5) consists of a set of $3n$ decoupled second-order differential equations:

$$\ddot{v}_i + \omega_{n,i}^2 v_i = f_{v,i}, \tag{6}$$

with $i = 1, 2, \ldots, 3n$. Eqs. (6) are solved independently and then used to express the original vector $\boldsymbol{u}$ from the vector $\boldsymbol{v}$.

3. CASE STUDY: MECHANISM WITH TWO RIGID LINKS AND TWO FLEXIBLE HINGES

The mechanism of Fig. 2 consists of two rigid, heavy links and two straight-axis flexible hinges that can be either massless or heavy. All links are collinear. The rigid links have lengths L_1, L_2, and their constant cross-sections are assumed square with side lengths a_1, a_2. The flexible hinges' lengths are l_1, l_2, and their constant rectangular cross-sections have the dimensions w_1, h_1 and w_2, h_2. The mass centers C_1, C_2 of the rigid links are placed at the links' midpoints due to the links constant cross-sections. While the above assumptions allow to simplify the mathematical model, they are nonbinding, and the general mathematical model described in the previous section can be applied to mechanisms with noncolinear and variable cross-section links, for instance.

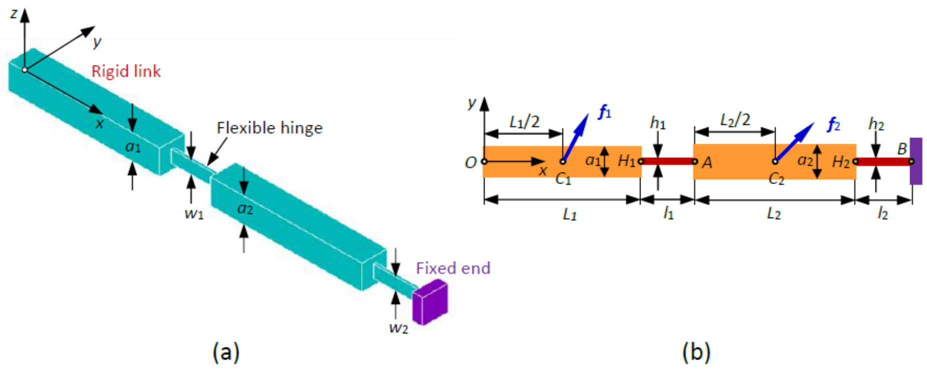

Fig. 2 – Collinear serial mechanism with two rigid links and two flexible hinges: a) three-dimensional view; b) Planar view.

The planar motion of the mechanism is defined by 6 DOF since each rigid link has 3 DOF. The displacement vector comprises the displacements at the rigid links centers C_1, C_2, and is therefore $\boldsymbol{u} = [\boldsymbol{u_1} \;\; \boldsymbol{u_2}]^T = [u_{1x} \;\; u_{1y} \;\; \theta_1 \; u_{2x} \;\; u_{2y} \;\; \theta_2]^T$. The mechanism mass matrix $\mathbf{M}$ and compliance matrix $\mathbf{C}$, which are both 6×6 matrices, are formulated next.

Mass matrix

It is assumed that both the rigid links and the flexible hinges are constructed from the same homogeneous material with mass density ρ. While the rigid links are heavy, the flexible hinges can be either massless or heavy, depending on their dimensions with respect to the rigid links dimensions. The mechanism mass matrix is formulated here for both instances.

a) Massless hinges. For massless hinges, the 6 x 6 mass matrix results directly from Eq. (1) for $n = 2$, namely:

$$\mathbf{M} = \begin{bmatrix} \mathbf{M}^{(1)} & \mathbf{0} \\ \mathbf{0} & \mathbf{M}^{(2)} \end{bmatrix} \quad \text{with} \quad \mathbf{M}^{(i)} = \mathbf{M}_r^{(i)} = \begin{bmatrix} m_i & 0 & 0 \\ 0 & m_i & 0 \\ 0 & 0 & J_i \end{bmatrix}, \tag{7}$$

where $i = 1, 2$, $\mathbf{0}$ is the 3×3 zero matrix, and the subscript "r" denotes the rigid links. The elements of the 3×3 submatrices forming $\mathbf{M}$ are: $m_i = \rho L_i(a_i)^2$ and $J_i = m_i(L_i)^2/12$.

b) Heavy hinges. When the hinge inertia is comparable to that of the rigid links, the mass submatrices of Eq. (7) are calculated as:

$$\mathbf{M}^{(i)} = \mathbf{M}_r^{(i)} + \mathbf{M}_h^{(i)}, \tag{8}$$

where $i = 1, 2$, and the subscript "h" denotes the flexible hinges.

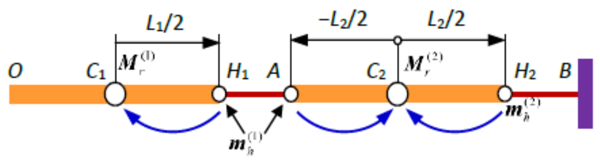

Fig. 3 – Schematic representation of mechanism with lumped masses.

As shown in Fig. 3 and as detailed in [25], the actual inertia of the hinge (1) can be lumped at its ends H_1 and A, and results in the following two identical submatrices:

$$\mathbf{m}_{h1}^{(1)} = \mathbf{m}_{h2}^{(1)} = \mathbf{m}_h^{(1)} = \begin{bmatrix} m_h^{(1)}/2 & 0 & 0 \\ 0 & m_h^{(1)}/2 & 0 \\ 0 & 0 & 0 \end{bmatrix} \text{ with } m_h^{(1)} = \rho l_1 w_1 h_1, \tag{9}$$

where $m_h^{(1)}$ is the mass of hinge (1). The inertia of hinge (2), which is fixed at the end B, is lumped at the moving end H_2 and is expressed by the matrix (see also details in [25]):

$$\mathbf{m}_h^{(2)} = \begin{bmatrix} m_h^{(2)}/3 & 0 & 0 \\ 0 & 33m_h^{(2)}/140 & 0 \\ 0 & 0 & 0 \end{bmatrix} \text{ with } m_h^{(2)} = \rho l_2 w_2 h_2, \tag{10}$$

where $m_h^{(2)}$ is the mass of hinge (2). It should be noted that, instead of the lumped-parameter approach applied here, the consistent formulation (as in FEA) – see also

[25] – may also be used to calculate the hinge inertia at points H_1, A and H_2. The three submatrices of Eqs. (9) and (10) that account for the two hinges lumped inertia are transferred from the points H_1, A and H_2 to the points C_1 and C_2 respectively, as depicted in Fig. 3, which results in:

$$\mathbf{M}_h^{(1)} = \left(\mathbf{T}_{C_1H_1}\right)^T \mathbf{m}_h^{(1)}\mathbf{T}_{C_1H_1},$$
$$\mathbf{M}_h^{(2)} = \left(\mathbf{T}_{C_2A}\right)^T \mathbf{m}_h^{(1)}\mathbf{T}_{C_2A} + \left(\mathbf{T}_{C_2H_2}\right)^T \mathbf{m}_h^{(2)}\mathbf{T}_{C_2H_2}. \quad (11)$$

The translation matrices to C_1 and C_2 are:

$$\mathbf{T}_{C_1H_1} = \begin{bmatrix} 1 & 0 & 0 \\ 0 & 1 & 0 \\ 0 & -L_1/2 & 1 \end{bmatrix}, \ \mathbf{T}_{C_2A} = \begin{bmatrix} 1 & 0 & 0 \\ 0 & 1 & 0 \\ 0 & L_2/2 & 1 \end{bmatrix},$$
$$\mathbf{T}_{C_2H_2} = \begin{bmatrix} 1 & 0 & 0 \\ 0 & 1 & 0 \\ 0 & -L_2/2 & 1 \end{bmatrix}. \quad (12)$$

Compliance matrix

The displacements at C_1 and C_2 are calculated based on the two hinges compliance matrices and the generic force vectors $\boldsymbol{f}_1$, $\boldsymbol{f}_2$ acting at the same points, namely:

$$\boldsymbol{u}_1 = \left(\mathbf{C}_{C_1C_1}^{(1)} + \mathbf{C}_{C_1C_1}^{(2)}\right)\boldsymbol{f}_1 + \mathbf{C}_{C_1C_2}^{(2)}\boldsymbol{f}_2$$
$$\boldsymbol{u}_2 = \mathbf{C}_{C_2C_1}^{(2)}\boldsymbol{f}_1 + \mathbf{C}_{C_2C_2}^{(2)}\boldsymbol{f}_2 = \left(\mathbf{C}_{C_1C_2}^{(2)}\right)^T\boldsymbol{f}_1 + \mathbf{C}_{C_2C_2}^{(2)}\boldsymbol{f}_2 \quad \rightarrow$$
$$\underbrace{\begin{bmatrix} \boldsymbol{u}_1 \\ \boldsymbol{u}_2 \end{bmatrix}}_{\boldsymbol{u}} = \underbrace{\begin{bmatrix} \mathbf{C}_{C_1C_1}^{(1)} + \boldsymbol{C}_{C_1C_1}^{(2)} & \mathbf{C}_{C_1C_2}^{(2)} \\ \left(\mathbf{C}_{C_1C_2}^{(2)}\right)^T & \mathbf{C}_{C_2C_2}^{(2)} \end{bmatrix}}_{\mathbf{C}} \underbrace{\begin{bmatrix} \boldsymbol{f}_1 \\ \boldsymbol{f}_2 \end{bmatrix}}_{\boldsymbol{f}}. \quad (13)$$

Equation (13) is of the form $\boldsymbol{u} = \mathbf{C}\boldsymbol{f}$ and identifies the mechanism compliance matrix $\mathbf{C}$. The individual equations of Eq. (13) use the superposition principle since the system is linear. The displacement vector $\boldsymbol{u}_1$ at C_1, for instance, is the sum of two displacements generated by $\boldsymbol{f}_1$ when acting on the hinge (1) and the hinge (2), and a third displacement produced by $\boldsymbol{f}_2$ applied to the hinge (2); similarly, $\boldsymbol{u}_2$ generated at C_2 adds the displacement due to $\boldsymbol{f}_1$ acting along hinge (2) and the displacement along the same hinge under the action of $\boldsymbol{f}_2$. The subscripts of the compliance submatrices of Eq. (13) have the following significance: the first letter indicates the point with respect to which the matrices are calculated while the second letter indicates the point where the force is being applied at. The superscripts (1) and (2) identify the respective flexible hinge. These compliance matrices are determined based on the hinge compliance matrices $\mathbf{C}^{(1),}$ $\mathbf{C}^{(2)}$ of Eq. (2) and the related translation matrices as follows:

$$\begin{gathered}
\mathbf{C}_{C_1C_1}^{(1)}=\left(\mathbf{T}_{C_1H_1}\right)^T\mathbf{C}^{(1)}\mathbf{T}_{C_1H_1};\ \mathbf{C}_{C_1C_1}^{(2)}=\left(\mathbf{T}_{C_1H_2}\right)^T\mathbf{C}^{(2)}\mathbf{T}_{C_1H_2};\\
\mathbf{C}_{C_1C_2}^{(2)}=\left(\mathbf{T}_{C_1H_2}\right)^T\mathbf{C}^{(2)}\mathbf{T}_{C_2H_2};\\
\mathbf{C}_{C_2C_1}^{(2)}=\left(\mathbf{T}_{C_2H_2}\right)^T\mathbf{C}^{(2)}\mathbf{T}_{C_1H_2}=\left(\mathbf{C}_{C_1C_2}^{(2)}\right)^T;\mathbf{C}_{C_2C_2}^{(2)}=\left(\mathbf{T}_{C_2H_2}\right)^T\mathbf{C}^{(2)}\mathbf{T}_{C_2H_2}.
\end{gathered}\tag{14}$$

For the constant rectangular cross-section flexure hinges of this mechanism, the four compliances forming the compliance matrix $\mathbf{C}^{(i)}$ of Eq. (2) are: $C_x^{(i)} = l_i/(EA_i), C_{yy}^{(i)} = (l_i)^3/(3EI),\ C_{y\theta}^{(i)} = -(l_i)^2/(2EI), C_{\theta\theta}^{(i)} = l_i/(EI)$; the cross-section area and area moment of inertia are: $A_i = w_ih_i$ and $I_i = w_i(h_i)^3/12$.

Note that the particular form of the compliance matrix in Eq. (13) is consistent with the general compliance matrix of Eq. (2). The translation matrices $\mathbf{T}_{C_1H_1}$ and $\mathbf{T}_{C_2H_2}$ of Eq. (14) are defined in Eq. (12) while $\mathbf{T}_{C_1H_2}$ (see Fig. 3) is calculated as:

$$\mathbf{T}_{C_1H_2}=\begin{bmatrix}1 & 0 & 0\\ 0 & 1 & 0\\ 0 & -(L_1/2+l_1+L_2) & 1\end{bmatrix}.\tag{15}$$

Finite element analysis validation of analytical model

The analytical model accuracy was checked by comparing the model's 6 natural frequencies to those resulting from finite element simulation. Table 1 lists the geometric parameters of the design variants that were used for the analytical-numerical comparison. Without loss of generality, the designs have $a_1 = a_2 = a$, $l_1 = l_2 = l$, $w_1 = w_2 = w$, and $h_1 = h_2 = h$. Young's modulus is $E = 2\cdot10^{11}$ N/m^2 and the mass density is ρ = 7 800 kg/m^3. Three-dimensional elements were utilized in the ANSYS software for the FEA.

Table 1

Geometric dimensions (in m) of design variants

Design #	L_1	L_2	a	l	w	h
1	0.04	0.05	0.01	0.016	0.006	0.001
2	0.04	0.05	0.01	0.02	0.006	0.001
3	0.04	0.05	0.01	0.02	0.005	0.0008
4	0.06	0.05	0.01	0.02	0.005	0.0008
5	0.06	0.06	0.01	0.02	0.005	0.0008
6	0.06	0.06	0.02	0.02	0.005	0.0008

Table 2 displays the analytical and FEA natural frequency values for these design variants together with the relative errors. The analytical natural frequencies utilized the model with heavy flexible hinges when evaluating the overall mass matrix. When using consistent masses for the two flexible hinges, which entails inclusion of rotation effects, the resulting analytical-model natural frequencies were almost identical to those listed in Table 2 and which utilized lumped masses.

Table 2

Natural frequencies (in Hz) by analytical model (A), finite element analysis (FEA) simulation, and relative percentage errors (E in %)

Design #		ω_{n1}	ω_{n2}	ω_{n3}	ω_{n4}	ω_{n5}	ω_{n6}
1	A	20.81	161.38	939.44	1,753.70	4,580.79	11,465.20
	FEA	21.34	161.01	945.67	1.775.77	4,337.74	10,942.70
	E	2.48	0.19	0.66	1.25	5.30	4.56
2	A	17.52	137.55	706.61	1,347.87	4,097.19	10,254.80
	FEA	17.89	136.73	697.71	1,312.50	3,920.15	9,885.20
	E	2.07	0.60	1.26	2.62	4.32	3.6
3	A	11.50	90.19	462.49	880.74	3,364.24	8,426.07
	FEA	11.69	89.70	459.75	863.41	3,253.40	8,171.00
	E	1.63	0.54	0.59	1.97	3.29	3.03
4	A	8,59	66.69	410.28	795.16	2,908.07	7,928.3
	FEA	8.75	66.62	414.80	784.70	2,804.00	7,700.6
	E	1.83	0.10	1.09	1.32	3.57	2.86
5	A	7.87	60.11	382.48	719.08	2,842.20	7,419.57
	FEA	8.01	60.06	386.44	713.54	2,732.70	7,176.30
	E	1.75	0.08	1.02	0.77	3.85	3.28
6	A	3.96	30.22	192.16	359.73	1,433.60	3,750.44
	FEA	4.01	29.66	191.54	348.16	1,398.40	3,640.00
	E	1.25	1.85	0.32	3.22	2.46	2.94

The 6 mode shapes associated to the FEA natural frequencies corresponding to one of the 6 design variants are illustrated in Fig. 4. These graphic modes can be visually characterized by the specific way the two flexure hinges deform while undergoing free vibrations. As such, the first two mode shapes are bending ones (the flexible hinges deform in bending only), while the last two modes are purely axial (the flexible hinges undergo extension/compression solely). Modes 3 and 4 combine bending and axial deformations of the flexible hinges. It should be noted that the FEA mode shapes confirmed the eigenvectors that were calculated analytically. Each eigenvector is formed of the amplitudes of the individual harmonic vibrations along the mechanism 6 independent coordinates and is of the form $\boldsymbol{V}_i = [U_{1x,i}\ \ U_{1y,i}\ \ \Theta_{1,i}\ U_{2x,i}\ \ U_{2y,i}\ \ \Theta_{2,i}]^{\mathrm{T}}$, $i = 1, 2, \ldots, 6$, where the 6 amplitudes may be positive, negative or zero. Each of the FEA mode shapes of Fig. 4 is accompanied by its analytical symbolic eigenvector, which lists +, − or 0 for the 6 components, depending on the sign of a particular component in the analytical eigenvector.

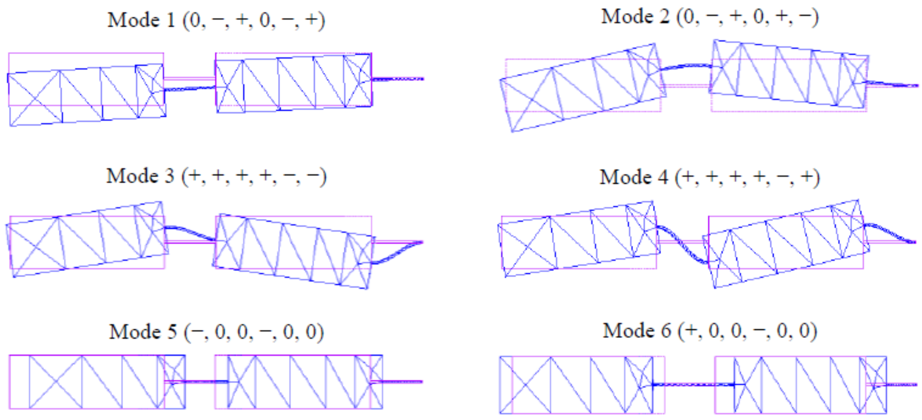

Fig. 4 – FEA mode shapes and analytical eigenvectors.

Influence of hinges' inertia on natural frequencies

A comparison was performed between the natural frequencies that result from the analytical models with and without hinge inertia included when varying the hinge lengths and cross-section dimensions. A base design was used with $L_1 = L_2 = 0.05$ m, $a_1 = a_2 = 0.01$ m, $l_1 = l_2 = l = 0.01$ m, $w_1 = w_2 = w = 0.006$ m, $h_1 = h_2 = h = 0.001$ m, $E = 2{\cdot}10^{11}$ N/m^2, and $\rho = 7800$ kg/m^3. The following ranges were used for the hinge parameters: $l \to [0.01; 0.05]$ m, $w \to [0.002; 0.01]$ m, and $h \to [0.0005; 0.002]$ m. The analysis revealed that all relative natural frequencies $\Delta\omega_{ni}/\omega_{ni}$ (where $\Delta\omega_{ni}$ represents the difference between the i^{th} natural frequency without inertia and the i^{th} natural frequency with hinge inertia) increased when l, w, and h assumed larger values. Figure 5 illustrates this conclusion by plotting the first relative natural frequency in terms of each of the three hinge parameters. As this figure shows, and as also confirmed by similar variations and ranges of the other relative natural frequencies, the deviations (errors) produced by ignoring the hinge inertia are small. The worst-case scenario results in a first relative natural frequency of 6.64% when $l = 0.05$ m, $w = 0.01$ m and $h = 0.002$ m.

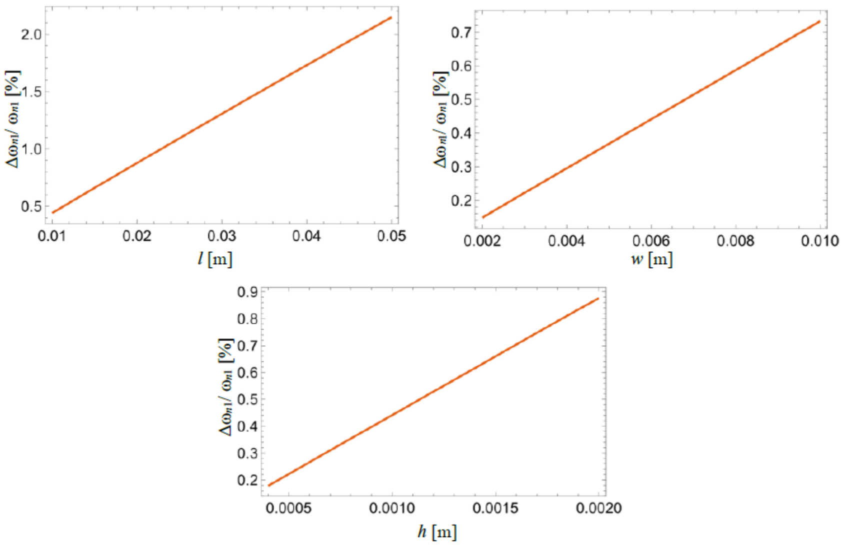

Fig. 5 – Relative first natural frequency plots in terms of the flexible hinges' dimensions.

Influence of geometric parameters on natural frequencies

The influence of the mechanism geometry on the natural frequencies was studied by using the base design of the previous section, and by varying each geometric parameter at a time. The following ranges were used for the hinge parameters: L_1, $L_2 \rightarrow$ [0.01; 0.08] m, a_1, $a_2 \rightarrow$ [0.005; 0.03] m, l_1, $l_2 \rightarrow$ [0.01; 0.05] m, w_1, $w_2 \rightarrow$ [0.005; 0.01] m, and h_1, $h_2 \rightarrow$ [0.0005; 0.002] m. All natural frequencies vary monotonically in terms of the 10 parameters; the natural frequencies are larger for smaller values of L_1, L_2, a_1, a_2, l_1, l_2, and for larger w_1, w_2, h_1, h_2. These trends are illustrated in Fig. 6 and Fig. 7 that plot the variation of the first natural frequency. For the parameter ranges selected here the extreme values of the first natural frequency are $\omega_{n1,\min} = 0.44$ Hz and $\omega_{n1,\max} = 1{,}042.28$ Hz.

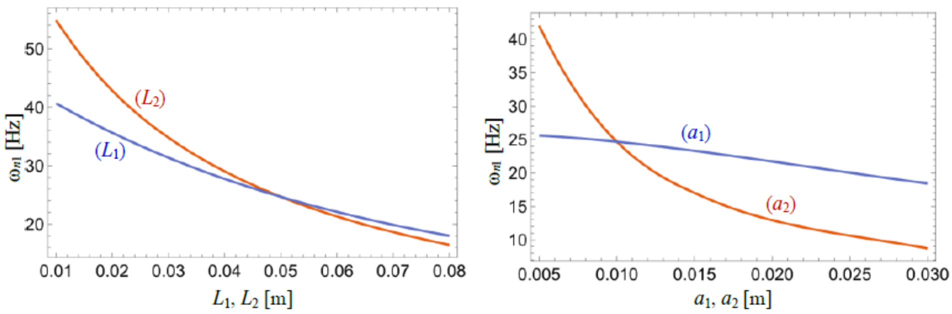

Fig. 6 – First natural frequency plots in terms of the rigid links' dimensions.

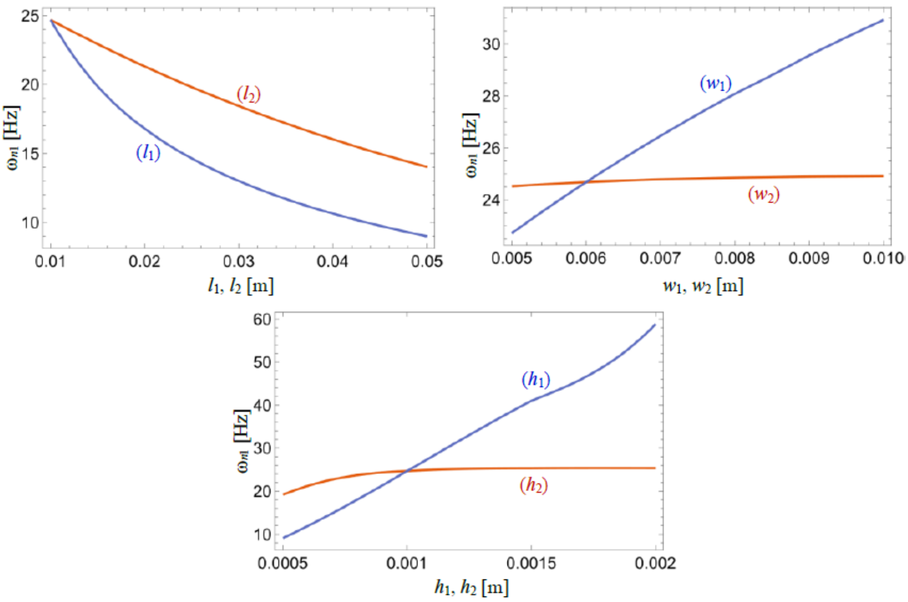

Fig. 7 – First natural frequency plots in terms of the flexible hinges' dimensions.

Vertical mechanism (double pendulum)

When the mechanism of Fig. 2 is placed with its axis vertical (and essentially becomes a pendulum – see also [28–30] for study of similar mechanisms' free-response dynamics), the gravity alters the compliance and, potentially, the system natural frequencies. This mechanism position also transforms the free system analyzed in the previous sections into a forced system. Figure 8 is the sketch of the deformed pendulum where the gravity forces act at the mass centers of the two rigid links C_1, C_2.

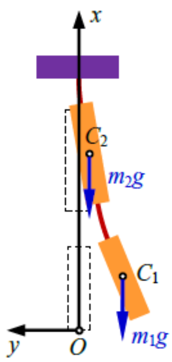

Fig. 8 – Flexible-hinge double pendulum with gravitational effects in vertical plane.

In addition to the two x-axis gravitational forces $-m_1 g$ and $-m_2 g$, two z-axis moments are produced by the two forces with respect to the mechanism fixed point, namely: $-(m_1 g)u_{1y}$ and $-(m_2 g)u_{2y}$ where m_1, m_2 are the lumped masses and u_{1y}, u_{2y} are the horizontal deflections (force arms) at the centers C_1, C_2. Given the mechanism DOF sequence, the force vector $\boldsymbol{f} = [-m_1 g \;\; 0 \;\; -(m_1 g)u_{1y} \;\; -m_2 g \;\; 0 \;\; -(m_2 g)u_{2y}]^{\mathrm{T}}$ is formed, which can be written as $\boldsymbol{f} = \boldsymbol{f_r} + \boldsymbol{f_t}$ with the rotation portion being $\boldsymbol{f_r} = [0 \;\; 0 \;\; -(m_1 g)u_{1y} \;\; 0 \;\; 0 \;\; -(m_2 g)u_{2y}]^{\mathrm{T}}$ and the translation term being $\boldsymbol{f_t} = [-m_1 g \;\; 0 \;\; 0 \;\; -m_2 g \;\; 0 \;\; 0]^{\mathrm{T}}$. The rotation force vector is expressed as:

$$\boldsymbol{f_r} = \underbrace{\begin{bmatrix} 0 & 0 & 0 & 0 & 0 & 0 \\ 0 & 0 & 0 & 0 & 0 & 0 \\ 0 & -m_1 g & 0 & 0 & 0 & 0 \\ 0 & 0 & 0 & 0 & 0 & 0 \\ 0 & 0 & 0 & 0 & 0 & 0 \\ 0 & 0 & 0 & 0 & -m_2 g & 0 \end{bmatrix}}_{\mathbf{K_g}} \underbrace{\begin{bmatrix} u_{1x} \\ u_{1y} \\ \theta_1 \\ u_{2x} \\ u_{2y} \\ \theta_1 \end{bmatrix}}_{\boldsymbol{u}} \quad \text{or} \quad \boldsymbol{f_r} = \mathbf{K_g}\boldsymbol{u} \tag{16}$$

where $\mathbf{K_g}$ represents the stiffness matrix due to gravitational effects. The generic Eq. (5) becomes:

$$\begin{gathered} \mathbf{M}\ddot{\boldsymbol{u}} + \mathbf{C}^{-1}\boldsymbol{u} = \boldsymbol{f_r} + \boldsymbol{f_t} \quad \text{or} \quad \mathbf{M}\ddot{\boldsymbol{u}} + \mathbf{C}^{-1}\boldsymbol{u} = \mathbf{K_g}\boldsymbol{u} + \boldsymbol{f_t} \;\rightarrow \\ \mathbf{M}\ddot{\boldsymbol{u}} + \underbrace{\left(\mathbf{C}^{-1} - \mathbf{K_g}\right)}_{\mathbf{C}_{\mathbf{eq}}^{-1}}\boldsymbol{u} = \boldsymbol{f_t} \end{gathered} \tag{17}$$

$\mathbf{C_{eq}} = (\mathbf{C}^{-1} - \mathbf{K_g})^{-1}$ is the equivalent compliance matrix that includes gravitational effects in addition to the flexible hinges' elastic properties. The equation governing the free response of the pendulum results from Eq. (17) for $\boldsymbol{f_t} = \mathbf{0}$, which is:

$$\mathbf{M}\ddot{\boldsymbol{u}} + \underbrace{\left(\mathbf{C}^{-1} - \mathbf{K_g}\right)}_{\mathbf{C}_{\mathbf{eq}}^{-1}}\boldsymbol{u} = \mathbf{0} \;\rightarrow\; \mathbf{D_{eq}} = \left(\mathbf{C_{eq}}\mathbf{M}\right)^{-1}. \tag{18}$$

As per Eq. (18), a new dynamic matrix $\mathbf{D_{eq}}$ must be used to account for the rotation effect of gravity. The natural frequencies of the designs described in Table 1 were calculated again by means of $\mathbf{D_{eq}}$; the results (which are not included in Table 2) were very close to the ones generated by $\mathbf{D}$ (when the mechanism of Fig. 2 is placed in a horizontal plane and the gravitational effects are eliminated) with relative errors less than 1%. This suggests that, at least for the analyzed design variants, the effect of gravity can be ignored when the mechanism is placed with its axis vertical.

The forced response of the flexible pendulum can be analyzed by using the modal superposition method described in Eqs. (5) and (6). For a mechanism defined by L_1 = 0.04 m, L_2 = 0.05 m, $a_1 = a_2$ = 0.01 m, $l_1 = l_2$ = 0.02 m, $w_1 = w_2$ = 0.006 m, $h_1 = h_2$ = 0.001 m, $E = 2\cdot10^{11}$ N/m^2, ρ = 7800 kg/m^3, and the nonzero initial conditions $\theta_1(0) = 8^o$, $\theta_2(0) = -5^o$, Fig. 9 plots the time variations of the two rigid links rotation angles θ_1 and θ_2.

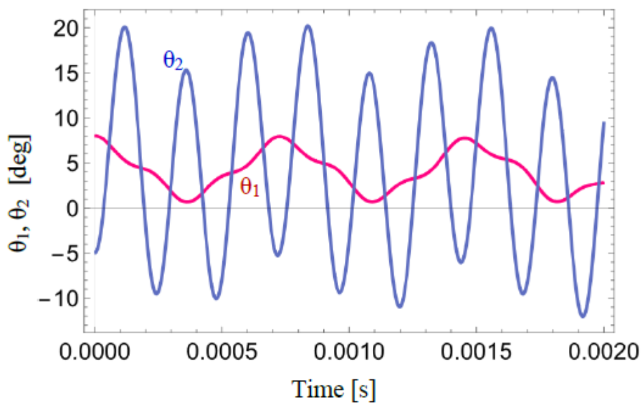

Fig. 9 – Time plots of double pendulum's rigid links rotation angles.

4. CONCLUSIONS

A lumped-parameter analytical matrix method is presented that models the dynamics of serial planar free-fixed mechanisms with rigid links and flexible hinges. The method selects the minimum number of degrees of freedom of the rigid links and uses mass and compliance matrices to generate a linear eigenvalue problem enabling to easily calculate the in-plane natural frequencies. The model also evaluates the time response of the free/forced mechanism. The natural frequencies and mode shapes of a particular collinear mechanism are thoroughly analyzed in terms of the system geometry. The natural frequencies and the forced response of the mechanism that is placed vertically, when it becomes a double pendulum, are also evaluated.

Received on June 5, 2025

REFERENCES

1. SHABANA, A.A., *Dynamics of Multibody Systems*, Cambridge University Press, New York, 2010.
2. RUI, X., WANG, J., ZHANG, J., *Transfer Matrix Method for Multibody Systems: Theory and Applications*, John Wiley & Sons, New York, 2018.
3. YANG, T.Y., *Finite Element Structural Analysis*, McGraw-Hill, New York, 1986.

4. CLEGHORN, W.L., FENTON, R.G., TABARROK, B., *Finite Element Analysis of High-Speed Flexible Mechanisms*, Mechanism and Machine Theory, **16** , *4*, pp. 407–424, 1981.
5. KITIS, L., LINDENBERG, R.K., *Natural Frequencies and Mode Shapes of Flexible Mechanisms by a Transfer Matrix Method*, Finite Elements in Analysis and Design, **6**, *4*, pp. 267–285, 1990.
6. HAC, M., *Dynamics of Flexible Mechanisms with Mutual Dependence Between Rigid Body Motion and Longitudinal Deformation of Links*, Mechanism and Machine Theory, **30,** *6*, pp. 837 – 847, 1995.
7. SRIRAM, B.R., MRUTHYUNJAYA, T.S., *Dynamics of Flexible-Link Mechanisms*, Computers and Structures, **56**, *6*, pp. 1029–1037, 1995.
8. FALLAHI, B., *An Enhanced Computational Scheme for Analysis of Elastic Mechanisms*, Computers and Structures, **62**, *2*, pp. 369–372, 1997.
9. WU, J.J., *Use of Elastic-and-Rigid-Combined Beam Element for Dynamic Analysis of a Two-Dimensional Frame with Arbitrary Distributed Rigid Beam Segments*, Applied Mathematical Modelling, **35**, pp. 1240–1251, 2011.
10. BANERJEE, J.R., *Dynamic Stiffness Formulation and its Application for a Combined Beam and a Two Degree-of-Freedom System*, Journal of Vibration and Acoustics, **125**, *3*, pp. 351–358, 2003.
11. OBRADOVIC, A. *et al*., *Free Vibration of Structures Composed of Rigid Bodies and Elastic Beam Segments*, Journal of Sound and Vibration, **347**, pp. 126–138, 2015.
12. LIU, X. *et al*., *An Exact Dynamic Stiffness Metod for Multibody Systems Consisting of Beams and Rigid Bodies*, Mechanical Systems and Signal Processing, **150**, pp. 107264-1 – 13, 2021.
13. RUI, X. *et al*., *Discrete Time Transfer Matrix Method for Multibody System Dynamics*, Multibody System Dynamics, **18**, *1*, pp. 317–344, 2005.
14. RUI, X. *et al*., *Transfer Matrix Method for Linear Multibody Systems*, Multibody System Dynamics, **19**, *3*, pp. 179–207, 2008.
15. HU, J., WEN, T., HE, J., *Dynamics of Compliant Mechanisms Using Transfer Matrix Method*, International Journal of Precision Engineering and Manufacturing, **21**, pp. 2173–2189, 2020.
16. LING, M. *et al*., *Modified Transfer Matrix Method for Vibration Analysis of Beam Structures Including Branches and Rigid Bodies*, Mechanical Systems and Signal Processing, **187**, pp. 109858-1 – 23, 2023.
17. WITTRICK, W.H., WILLIAMS, F.W., *A General Algorithm for Computing Natural Frequencies of Elastic Structures*, Journal of Mechanical Applied Mathematics, **24**, *3*, pp. 263–284, 1971.
18. WASFY, T.M., NOOR, A.K., *Computational Strategies for Flexible Multibody Systems*, Applied Mechanical Reviews, **56**, *6*, pp. 35–58, 2003.
19. SURDILOVIC, D., VUKOBRATOVIC, M., *One Method for Efficient Dynamic Modeling of Flexible Manipulators*, Mechanism and Machine Theory, **31**, *3*, pp. 297–315, 1996.
20. CUI, K., HAQUE, I., *Symbolic Equations of Motion for Hybrid Multibody Systems Using a Matrix-Vector Formulation*, Mechanism and Machine Theory, **32**, *6*, pp. 743–763, 1997.
21. HOPKINS, J.B., CULPEPPER, M.L., *Synthesis of Precision Serial Flexure Systems Using Freedom and Constraint Topologies (FACT)*, Precision Engineering, **35**, *4*, pp. 638–649, 2011.
22. LIEW, K. M., LEE, S. E., LIU, A. Q., *Mixed-Interface Substructures for Dynamic Analysis of Flexible Multibody Systems*, Engineering Structures, **18** , *7*, pp. 495–503, 1996.
23. ENGSTLER, C., KAPS, P., *A Comparison of One-Step Methods for Multibody System Dynamics in Descriptor and State Space Form*, Applied Numerical Mathematics, **24**, pp. 457–468, 1997.
24. ROSNER, M., LAMMERING, R., FRIEDRICH, R., *Dynamic Modeling and Model Order Reduction of Compliant Mechanisms*, Precision Engineering, **42**, pp. 85–92, 2015.
25. LOBONTIU, N., *Compliant Mechanisms: Design of Flexure Hinges*, 2nd ed., CRC Press, Boca Raton, FL, 2021.
26. MEIROVITCH, L., *Principles and Techniques of Vibrations*, Prentice-Hall, Englewood Cliffs, NJ, 1997.

27. RUBINSTEIN, M.F., *Matrix Computer Analysis of Structures*, Prentice-Hall, Englewood Cliffs, NJ, 1966.
28. DOLFO, G., VIGUÉ, J., *A More Accurate Theory of a Flexible-Beam Pendulum*, American Journal of Physics, **83**, pp. 525–530, 2015.
29. CHIROIU, V. *et al*., *On the Double Pendulum Flexible Manipulator*, Romanian Journal of Mechanics, **5**, *1*, pp. 52–60, 2020.
30. LOBONTIU, N., *Distributed-Parameter Dynamic Model and Optimized Design of a Four-Link Pendulum with Flexure Hinges*, Mechanism and Machine Theory, **36**, pp. 653 – 669, 2001.